Struct Multidisc Optim (2008) 36:493–507
DOI 10.1007/s00158-007-0184-5

INDUSTRIAL APPLICATION

Integrated design optimization of base-isolated concrete buildings under spectrum loading

X. K. Zou

Received: 12 May 2006 / Revised: 27 June 2007 / Accepted: 30 August 2007 / Published online: 12 April 2008
© Springer-Verlag 2008

Abstract Base isolation has become a practical control strategy for protecting structures against seismic hazards. Most previous studies on the optimum design of base-isolated structures have been focused on the design optimization of either the base isolation or the superstructure. It is necessary to simultaneously optimize both the base isolation and the superstructure as a whole to seek the most cost-efficient design for such structures. This paper presents an effective numerical optimization technique for the seismic design of base-isolated concrete building structures under spectrum loading. Attempts have been made to automate the integrated spectrum analysis and design optimization procedure and to minimize the total cost of the base-isolated building subject to design performance criteria in terms of the interstory drifts of the superstructure and the lateral displacement of the isolation system. In the optimal design problem formulation, the cost of the superstructure can be expressed in terms of concrete member sizes while assuming all these members to be linearly elastic under earthquake actions. However, the isolation system is assumed to behave nonlinearly, and its cost can be related to the effective horizontal stiffness of each isolator. Using the principle of virtual work, the lateral drift responses of concrete base-isolated buildings can be explicitly formulated and the integrated optimization problem can be solved by the optimality criteria method. The technique is capable of achieving the optimal balance between the costs of the superstructure and the isolation system while the design performance criteria can be simultaneously satisfied. One practical building example with and without base isolation is used to illustrate the effectiveness of the optimal design technique.

Keywords Response spectrum analysis · Structural optimization · Optimality criteria method · Principle of virtual work · Drift design · Base isolation · Base isolator

X. K. Zou (✉)
Ove Arup & Partners Hong Kong Ltd,
Level 5 Festival Walk, 80 Tat Chee Avenue,
Kowloon Tang, Kowloon,
Hong Kong, People's Republic of China
e-mail: connie.zou@arup.com; cezxk@yahoo.com

1 Introduction

Seismic isolation, an innovative seismic design approach, has been increasingly used in earthquake-prone regions for protecting structures against damage from earthquakes by limiting the earthquake attack, rather than resisting it (Booth 1994; Chopra 1995; Zhou 1997; Kelly 1997, 1999a, b; Komodromos 2000). Numerical studies (Shenton and Lin 1993) show that better performances of base-isolated reinforced concrete (RC) frames can be achieved when compared with fixed-base frames. Because the base isolation system can maintain the superstructure in the elastic range during earthquakes, it is very applicable for some important buildings, such as nuclear power plants, historical buildings, and laboratories with sensitive equipments. There have been many successful examples of base-isolated construction in the USA, Chile, Indonesia, New Zealand, Italy, China, and Japan (Kelly 1997). Unlike traditional fixed-base structures, a base-isolated structure includes the cost of an isolation system, but this additional cost can usually be offset by the cost saving in the superstructure because a well-designed base isolation system can largely reduce earthquake loading transferred to the

superstructure. More importantly, long-term savings are ensured because of better seismic performance by isolating the structure from seismic actions (Zhou 1997; Skinner et al. 1993; Ceccoli et al. 1999). It is believed that incorporating base isolators into initial building designs with simultaneous consideration of structure and isolation systems will bring better and more economical designs to engineers.

Traditionally, the superstructure and the isolation system are designed separately in a building. The determination of the satisfactory dynamic responses fulfilled in both the superstructure and the isolation system requires a highly iterative trial-and-error reanalysis and redesign process even with the aid of today's computer analysis software. Optimization of the base isolation system alone has been studied by many researchers (Zhou 1997; Constantinou and Tadjbakhsh 1985; Inaudi and Kelly 1993; Kelly 1999a; Fujita et al. 1994). However, most of these research efforts are not based on the cost of isolation system; instead, the focus has been on the determination of isolation parameters for the best structural performance index, which belongs to the scope of structural control or optimal control. Furthermore, few researchers (Cheng and Li 1996) adopted the integrated optimization approach for the design of a structure and associated control system. It is desirable to use all design resources of the structure and control systems because of strong interaction between the two systems so that simultaneous structure/control design is necessary to achieve ideal control effectiveness with minimum cost (Cheng and Li 1996). Therefore, it is intended in this research that both the structure and the base isolation, as a whole, are simultaneously optimized to achieve optimal performance design.

Structural and nonstructural damages caused by an earthquake excitation are mainly manifested through the control of story drift responses of the structure (Komodromos 2000). Lateral drift has been an important indicator that measures the level of damage to the structural and nonstructural components of a building; however, the control of drift performance is one of the most challenging and difficult tasks in building design because lateral drift is a system design criterion that requires the consideration of all structural members in a building structure (Chan et al. 1995; Chan 2001). Zou (2002), Zou and Chan (2005a) proposed a seismic drift performance design optimization of RC buildings subjected to earthquake loadings, such as response spectrum and time history loadings. Zou (2002), Chan and Zou (2004), and Zou and Chan (2005b) further studied the optimization technique for seismic inelastic drift design of buildings using nonlinear pushover analysis to meet the emerging trend of a performance-based design of structural systems. Zou (2006) and Zou et al. (2007a) developed a multiobjective optimization technique that incorporates the performance-based seismic design methodology of concrete building structures. Zou et al. (2007b) also performed more research on optimization of seismic retrofit design of RC structures when the retrofit strategy is confinement of the columns with fiber-reinforced polymer jackets. Zou (2002) further integrated design optimization with reliability analysis to develop the more rational reliability-based design optimization. However, these design optimization studies focused on traditional fixed-base building structures. Much effort is still needed to extend the current optimization technique to seismic design of multistory base-isolated building structures (Zou 2002; Zou and Chan 2001, 2004).

The seismic response of a base-isolated structure is usually investigated by two alternative approaches, i.e., making use of full nonlinear analysis (e.g., nonlinear time history analysis) or linearized techniques (e.g., response spectrum analysis; Kelly 1997). The response spectrum analysis, as a linear elastic analysis method, can provide approximate results that are sufficiently accurate (Chopra 1995) for a linear or nonlinear base-isolated structure, and thus it is still recommended to use in design codes (e.g., the Uniform Building Code, International Conference of Building Officials 1997) of a seismic-isolated structure for preliminary design. A nonlinear isolated structure is very often modeled assuming a bilinear behavior for the isolation system, which can be linearized by an effective stiffness and an effective damping coefficient.

This paper focuses on presenting an effective optimization technique for the drift performance design of RC building structures with base isolation. Attempts have been made to automate the integrated response spectrum analysis and design an optimization process (Zou 2002; Zou and Chan 2001, 2004). It is required that the natural vibration period of a base-isolated structure reaches a target period under specified earthquake loading and the lateral displacement of the isolation system be limited within the deformation capacity of individual isolators. It is also required that under specified earthquake loading, the interstory drift ratios of the superstructure can be controlled within an allowable range. Using the principle of virtual work, the lateral drift responses of the superstructure and the isolation system can be explicitly formulated in terms of the design variables. A rigorously derived optimality criteria (OC) method is developed to minimize the total construction cost of a base-isolated building structure subject to the interstory drifts of the superstructure, member sizing constraints, and the lateral displacement of the isolation system as well as effective stiffness constraints for the base isolation system. A ten-story, two-bay building example is used to illustrate the efficiency and practicality of the proposed optimization method, which is considered with and without base isolation. It is believed that this study will represent the starting point for future research on

effectiveness of the base-isolation system for optimal building seismic designs using nonlinear time history analysis (Zou and Chan 2004).

2 Seismic design optimization problem

2.1 Optimal design problem

2.1.1 Isolation system

A base-isolated concrete building structure consists of base isolation and superstructure systems. The isolation system includes all individual isolators that are linear or nonlinear. In the analysis, the bilinear behavior of a nonlinear isolator may be linearized by effective stiffness and effective damping (Komodromos 2000; International Conference of Building Officials 1997). As shown in Fig. 1a, a linear isolator results in a linear relationship of force and deflection, whereas a nonlinear isolator, normally modeled by a bilinear curve, exhibits a nonlinear relationship of force and deflection as shown in Fig. 1b. As displayed in Fig. 1c, each base isolator has the vertical stiffness, K^{v}, in the vertical direction and the horizontal effective stiffness, $K^{\mathrm{h}}_{\mathrm{eff}}$, in the transverse direction. The horizontal effective stiffness, $K^{\mathrm{h}}_{\mathrm{eff}}$, also called the secant stiffness, is defined to be the slope of a line from points O to B as shown in Figs. 1a and b. Summing up the individual horizontal

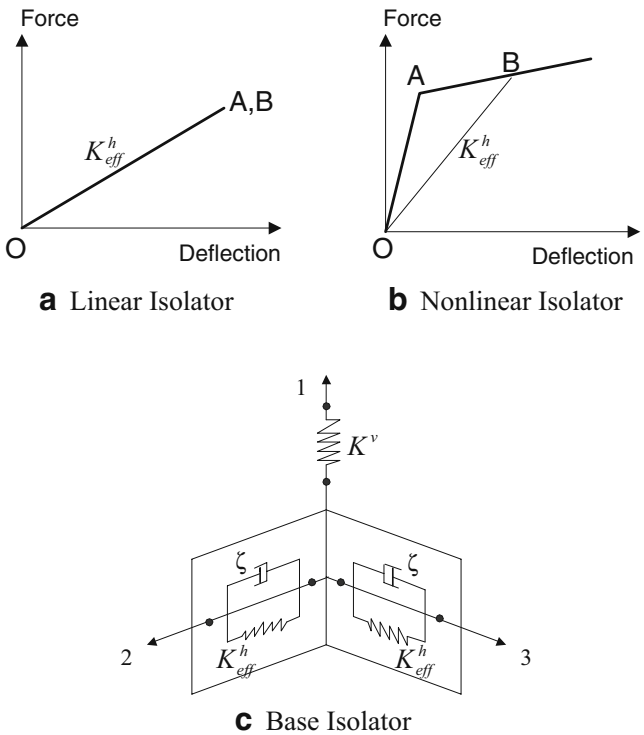

Fig. 1 **a–c** Definition of a linear and nonlinear isolator

effective stiffnesses, the lateral stiffness, K_B, of an isolation system having b=1,2,…,N_b isolators can be expressed as

$$K_B = \sum_{b=1}^{N_b} K^{\mathrm{h}}_{\mathrm{eff},b} \tag{1}$$

In general, the superstructure damping has a negligible effect on the damping of the first mode vibration of a base-isolated structure, and consequently, the structure damping is essentially the damping of the base-isolated system, which is dependent on the damping of isolators (Zhou 1997; Skinner et al. 1993; Kelly 1999a; International Conference of Building Officials 1997). The total effective damping of the isolation system damping, ζ_B, can be expressed collectively as (Kelly 1999b)

$$\zeta_B = \frac{1}{K_B} \sum_{b=1}^{N_b} K^{\mathrm{h}}_{\mathrm{eff},b} \zeta_b \tag{2}$$

where ζ_b is the effective damping ratio of the individual bth isolator with an effective stiffness equal to $K^{\mathrm{h}}_{\mathrm{eff},b}$. The design spectrum with the total effective damping, ζ_B, will be used in spectrum analysis.

2.1.2 Design variables

In this study, the number and type of isolators (linear and nonlinear) are predefined in the isolation system, and thus design variables are generally the vertical stiffness, K^{v}, and the horizontal effective stiffness, $K^{\mathrm{h}}_{\mathrm{eff}}$, of each base isolator. In general, the vertical stiffness K^{v} can be assumed to be linearly related to $K^{\mathrm{h}}_{\mathrm{eff}}$ such that $K^{\mathrm{v}} = n^{\mathrm{v}} K^{\mathrm{h}}_{\mathrm{eff}}$, where n^{v} is the stiffness ratio, which can be determined by statistical analysis. As a result, $K^{\mathrm{h}}_{\mathrm{eff}}$ can be considered as a primary design variable for an isolator.

If the topology and layout of the superstructure system is predefined, the structural member sizes can be generally taken as design variables of the superstructure. Given with a framework element of the six cross-sectional properties, i.e., the axial area (A_X), two shear areas (A_Y and A_Z), and three moment of inertias (I_X, I_Y, I_Z), these can be theoretically considered as basic design variables (Chan 2001). However, structural members for practical structures are generally not freely independent of each other. Assuming rectangular concrete members (see Fig. 2), their sectional properties can be expressed in terms of the width (B) and depth (D) as basic design variables as follows (Chan 2001).

$$A_X = B \times D; \quad A_Y = A_Z = \tfrac{5}{6} B \times D \tag{3a, b}$$

$$I_Y = \frac{1}{12} B^3 \times D; \; I_Z = \frac{1}{12} B \times D^3; \; I_X = \kappa B^3 \times D \tag{3c, d, e}$$

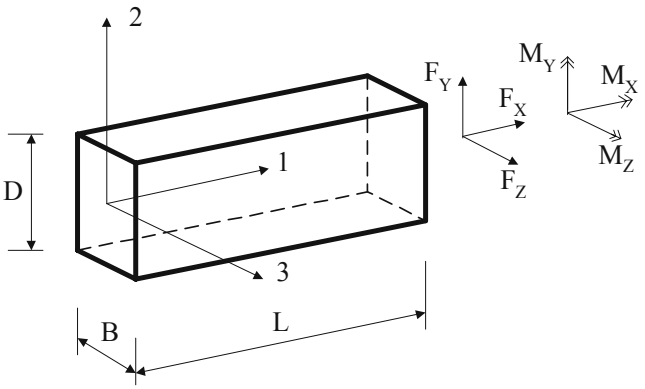

Fig. 2 Definition of local coordinate system for a structural member

where κ denotes the torsional coefficient that depends on the ratio value of depth to width (i.e., D/B) of member i. For other typical rectangular section, κ can be approximately set to 0.2.

2.1.3 Objective function

For a base-isolated concrete building having b=1, 2, 3,…, N_b base isolators and i=1, 2, 3,…, N_i members, there is only one independent sizing variable ($K^{\mathrm{h}}_{\mathrm{eff},b}$) for each base isolator, while concrete members generally have two independent sizing variables (B_i, D_i). The design optimization objective addressed herein is to minimize the construction cost involving the costs of the base isolation and the superstructure.

$$F\left(B_i, D_i, K^{\mathrm{h}}_{\mathrm{eff},b}\right) = \sum_{i=1}^{N_i} w_i B_i D_i + \sum_{b=1}^{N_b} f\left(K^{\mathrm{h}}_{\mathrm{eff},b}\right) \tag{4}$$

where F represents the total construction cost; the first part of the cost is the concrete cost not including the cost of reinforcing rebars because the variation of steel reinforcement is insensitive to lateral elastic displacement and w_i is the cost coefficient for the ith member of the superstructure; the second part is the isolation system cost, and $f\left(K^{\mathrm{h}}_{\mathrm{eff},b}\right)$ represents the cost of the bth base isolator, which can be assumed to be linearly related to the horizontal stiffness of each base isolator, $K^{\mathrm{h}}_{\mathrm{eff},b}$, as follows.

$$f\left(K^{\mathrm{h}}_{\mathrm{eff},b}\right) = m_1 K^{\mathrm{h}}_{\mathrm{eff},b} + m_2 \tag{5a}$$

where m_1 and m_2 are the cost coefficients of the bth base isolator, which can be obtained through a statistical investigation. Based on the discrete cost data provided from the manufacturer, the relationship between the cost and the effective horizontal stiffness of each type of isolator can be established and expressed in the form of a linear function by regression. As a result, the cost coefficients, m_1 and m_2, given in (5a) can then be found. In this study, rubber isolators are adopted because they are widely used in engineering practice; the cost data of various types of rubber isolators were provided by Shantou Vibro Tech Industrial and Development (Shantou, Guangdong Province, China). GZP-V5A series for linear isolators and GZY-V5A for nonlinear isolators are shown in Table 1 where χ_b represents the allowable deformation limit for each base isolator.

Based on the discrete cost data for GZP-V5A series shown in Table 1, the relationship between the cost and horizontal effective stiffness of each isolator is established and then is transformed into a linear continuous function by regression and m_1=4.4 and m_2=−2,087 are obtained, as shown in Fig. 3. As a result, the cost function of linear isolator can be approximately expressed by

$$f\left(K^{\mathrm{h}}_{\mathrm{eff},b}\right) = 4.4K^{\mathrm{h}}_{\mathrm{eff},b} - 2,087 \tag{5b}$$

Similarly, as shown in Fig. 4, the cost of nonlinear isolators for the GZY-V5A series can be approximately expressed by a series of linear functions as

$$\begin{aligned} f\left(K^{\mathrm{h}}_{\mathrm{eff},b}\right) &= 0.79K^{\mathrm{h}}_{\mathrm{eff},b} - 353.84(\mathrm{US\$})\left(450 \le K^{\mathrm{h}}_{\mathrm{eff},b} < 2,755\right) \\ &= 8.86K^{\mathrm{h}}_{\mathrm{eff},b} - 22370.00(\mathrm{US\$})\left(2,755 \le K^{\mathrm{h}}_{\mathrm{eff},b} < 3,210\right) \\ &= 2.23K^{\mathrm{h}}_{\mathrm{eff},b} - 1350.20(\mathrm{US\$})\left(3,210 \le K^{\mathrm{h}}_{\mathrm{eff},b} \le 4,490\right) \end{aligned} \tag{5c}$$

From the cost functions of linear and nonlinear isolators, a nonlinear isolator is found to be more cost effective than a linear isolator.

Table 1 Properties of rubber isolators

Isolator type	$K^{\mathrm{h}}_{\mathrm{eff}}$ (kN/m)	Cost (US$)	χ_b (m)
GZY300V5A	1,555	700	0.165
GZY350V5A	1,585	980	0.193
GZY400V5A	2,375	1,190	0.206
GZY500V5A	2,755	2,020	0.275
GZY600V5A	2,965	3,610	0.330
GZY700V5A	3,020	4,750	0.385
GZY800V5A	3,210	6,000	0.440
GZY900V5A	3,905	6,870	0.459
GZY1000V5A	4,490	8,890	0.480
GZP300V5A	495	685	0.165
GZP350V5A	755	962	0.193
GZP400V5A	965	1,160	0.206
GZP500V5A	1,100	1,966	0.275
GZP600V5A	1,190	3,505	0.330
GZP700V5A	1,455	4,639	0.385
GZP800V5A	1,765	5,886	0.440
GZP900V5A	2,225	6,726	0.459
GZP1000V5A	2,630	8,722	0.480

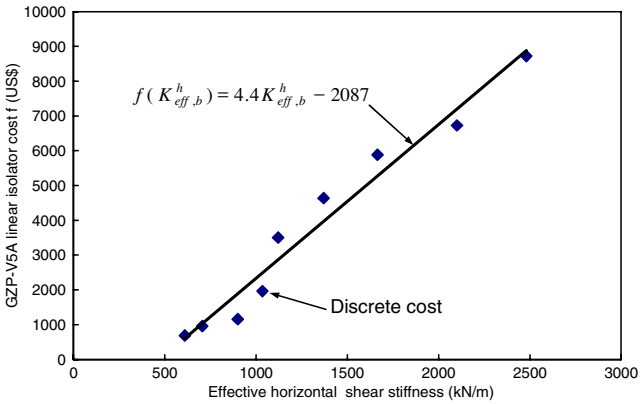

Fig. 3 Cost function of linear isolators GZP-V5A

2.1.4 Target period and displacement constraint at base story

The aim of base isolation is to reduce the force imparted to the structure to such a level that no damage to the structure or nonstructural elements occurs. For this purpose, there is usually a good separation between the fixed-base period of vibration, T_f, and the base-isolated period of vibration, T_B, for a building structure. Because of the low stiffness of the isolation system as compared to the superstructure, large lateral deformation is expected to concentrate at the base isolation level of a building such that the flexibility of the isolated structure is more affected by the base isolation while the superstructure behaves as essentially rigid. As a result, the fundamental natural period of the isolated structure can be assumed to be very much dominated by the stiffness of the isolation system and the total mass of the superstructure (Chopra 1995; Kelly 1999b).

In common practice of the base-isolated design, the design process starts with the preliminary design of a fixed-base structure. In general, it is desirable to devise a base isolation system that reduces the earthquake base shear by approximately at least three times of that of the fixed-base structure. Based on a given design spectrum for a building, the target base-isolated period of vibration, T_B, can be obtained approximately by dividing the acceleration value of the fixed-base structure by a factor of three (International Conference of Building Officials 1997). The Uniform Building Code (International Conference of Building Officials 1997) gives a recommendation on the amplitude of T_B that the isolation period of the structure may be greater than three times the elastic, fixed-base period of the structure above the isolation system under moderate earthquake loading.

Once the target period of the isolation system, T_B, is established, the main effort is then to design the isolation system so as to achieve the target period. Under the condition that the isolation system damping is temporarily fixed, the target period of the isolation system, T_B, can be achieved by controlling lateral seismic displacement at base floor level. Specifically, to attain sufficient flexibility so as to lengthen the period of the base isolation system, the isolation system is required to deform to maintain a minimum lateral displacement at the base floor level as follows.

$$u_0 \geq \delta_0^L \tag{6}$$

where u_0 is the lateral displacement at the top of the isolation system under the seismic loading; the subscripts 0 and L represents the base floor level and the lower limit value, respectively; δ_0^L is the specified minimum lateral displacement and can be given as

$$\delta_0^L = \Gamma^{(1)}\phi_0^{(1)}S_d^{(1)} \tag{7}$$

where $\Gamma^{(1)}$ is the modal participation factor for the first mode, $\phi_0^{(1)}$ is the amplitude of the first mode at base story, and $S_d^{(1)}$ is the spectral displacement for the first mode. Because the modal spectral displacement, $S_d^{(1)}$, can be related to the modal spectral acceleration, $S_a^{(1)}$, the minimum lateral displacement, δ_0^L, given in (7) can be rewritten as

$$\delta_0^L = \Gamma^{(1)}\phi_0^{(1)}\left(\frac{T_B}{2\pi}\right)^2 S_a^{(1)}(T_B,\zeta_B) \tag{8}$$

where $S_a^{(1)}(T_B,\zeta_B)$ with the damping ratio, ζ_B, can be obtained by

$$S_a(T_B,\zeta_B) = RS_a(T_B,\zeta = 5\%) \tag{9}$$

where T_B is the natural period of the base isolation system, $S_a(T_B,\zeta = 5\%)$ represents the spectral acceleration with 5% damping ratio, and R is a damping response reduction coefficient (Hart and Wong 2000).

Because base isolators are very flexible under lateral forces, it is necessary to prevent them from failure in the event of severe earthquakes. In addition to the design requirement on the minimum target period of the base isolation system, it is needed to ensure that each individual isolator does not deform excessively beyond the shear deformation capacity of the isolator (National Standard of the People's Republic of China 1994). Therefore, the

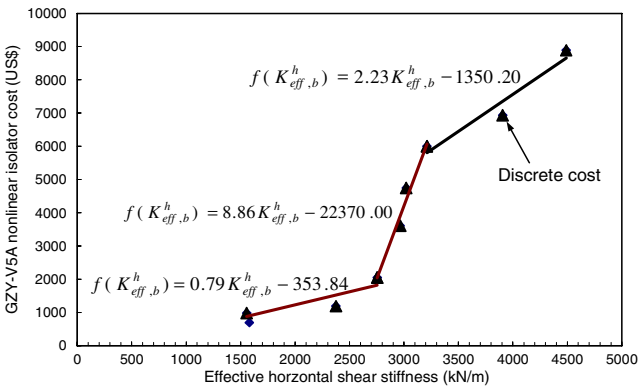

Fig. 4 Cost function of nonlinear isolators GZY-V5A

displacement of the isolation system at the base floor level, u_0, should be limited within the least allowable deformation capacity among all base isolators of the isolation system as

$$u_0 \le \delta_0^U \tag{10a}$$

where

$$u_0 \le \delta_0^U = \min_b(\chi_b) \tag{10b}$$

In (10a) and (10b), the superscript U represents the upper limit value, u_0^U is the upper bound displacement limit at the base floor level, and χ_b is the allowable deformation limit for each base isolator.

2.1.5 Lateral interstory drift constraint at the superstructure

As stated earlier, the lateral interstory drift of a multistory building is an important parameter that measures the damage level of the building under earthquake loading. If the differential lateral displacement of two adjacent story levels exceeds certain acceptable limit, the building will not satisfy the specified performance criterion. Therefore, a set of interstory drift constraints can be stated as follows.

$$\Delta u_j = u_j - u_{j-1} \le \delta_j^U \left(j = 1, 2, 3, \ldots, N_j\right) \tag{11}$$

where Δu_j is the interstory drift at the two adjacent jth and $j-1$th floor levels and u_j^U is the corresponding interstory drift limit value.

2.1.6 Member strength constraints

In addition to drift responses of an isolated building, each of the building members must be designed to ensure for adequate strength requirements (Paulay and Priestley 1992). That is,

$$\sigma_i \le \sigma_i^U (i = 1, 2, 3, ..., N_i) \tag{12}$$

where σ_i represents a stress state for member i and σ_i^U denotes the corresponding allowable member strength. To reduce computational effort, the strength design of a member can be considered separately on a member-by-member manner and therefore not included as part of the system design constraints on lateral drift performance. In general, after each structural analysis, the strength sizes of each structural member can be first sized in accordance with code requirements, and these values are then taken as the lower size bounds in the drift design optimization.

2.2 Formulation of optimal design

To facilitate numerical solutions of the design optimization problem, the implicit constraints in (6), (10a, b), and (11) should be expressed explicitly in terms of the design variables $K_{\text{eff},b}^{\text{h}}$, B_i, and D_i.

2.2.1 Lateral displacement formulation

In this study, the dynamic response considered is analyzed by the elastic response spectrum method. The dynamic structural responses in each mode are first determined, and then the peak responses are summed by statistically based combination rules. Based on the modal element internal forces obtained from the spectrum analysis, the principle of virtual work is employed to formulate all individual modal drift responses. Specifically, the total virtual work $u_j^{(n)}$ (i.e., the nth modal displacement at the jth level of a concrete building) involving the virtual work $u_{j,\text{isolator}}^{(n)}$ generated by isolators for base isolation and the virtual work $u_{j,\text{member}}^{(n)}$ produced by structural members for the superstructure can be written as

$$u_j^{(n)} = u_{j,\text{isolator}}^{(n)} + u_{j,\text{member}}^{(n)} \tag{13}$$

where

$$u_{j,\text{isolator}}^{(n)} = \sum_{b=1}^{N_b} \left(\frac{F_X^{(n)} f_{Xj}}{K_{\text{eff}}^v} + \frac{F_Y^{(n)} f_{Yj}}{K_{\text{eff}}^h} + \frac{F_Z^{(n)} f_{Zj}}{K_{\text{eff}}^h} \right)_b \tag{14}$$

$$u_{j,\text{member}}^{(n)} = \sum_{i=1}^{N_i} \int_o^{L_i} \left(\frac{F_X^{(n)} f_{Xj}}{EA} + \frac{F_Y^{(n)} f_{Yj}}{GA_Y} + \frac{F_Z^{(n)} f_{Zj}}{GA_Z} + \frac{M_X^{(n)} m_{Xj}}{GI_X} + \frac{M_Y^{(n)} m_{Yj}}{EI_Y} + \frac{M_Z^{(n)} m_{Zj}}{EI_Z} \right)_i \mathrm{d}x \tag{15}$$

where L_i is the length of member i; E and G are the axial and shear elastic material moduli; A_X, A_Y, and A_Z are the axial and shear areas for the cross-section; I_X, I_Y, and I_Z are the torsional and flexural moments of inertia for the cross-section; $F_X^{(n)}$, $F_Y^{(n)}$, $F_Z^{(n)}$, $M_X^{(n)}$, $M_Y^{(n)}$, and $M_Z^{(n)}$ are the nth modal member internal forces and moments; and f_{Xj}, f_{Yj}, f_{Zj}, m_{Xj}, m_{Yj}, and m_{Zj} are the virtual member forces and moments because of a unit virtual load applied to the building at the location corresponding to the displacement u_j. Note that the coordinate system and sign convention of member internal forces are depicted in Figs. 1c and 2.

Considering cylindrical isolators with the horizontal effective stiffness ($K_{\text{eff},b}^{\text{h}}$) taken as a design variable, the nth modal displacement $u_{j,\text{isolator}}^{(n)}$ shown in (14), which is deemed to zero for a structure without base isolation, can be simplified as

$$u_{j,\text{isolator}}^{(n)}\left(K_{\text{eff},b}^{\text{h}}\right) = \sum_{b=1}^{N_b} \left(\frac{C_{0bj}^{(n)}}{K_{\text{eff},b}^{\text{h}}} \right) \tag{16}$$

where

$$C_{0bj}^{(n)} = \frac{F_{Xb}^{(n)} f_{Xbj}}{n_{vb}} + \left(F_{Yb}^{(n)} f_{Ybj} + F_{Zb}^{(n)} f_{Zbj} \right) \tag{17}$$

Based on (16), the lateral displacement $u_0^{(n)}$ at the base story (i.e., j=0) is given as

$$u_0^{(n)}\left(K_{\mathrm{eff},b}^{\mathrm{h}}\right)=\sum_{b=1}^{N_b}\left(\frac{C_{0b0}^{(n)}}{K_{\mathrm{eff},b}^{\mathrm{h}}}\right) \tag{18}$$

Similarly, considering rectangular concrete members with the width (B_i) and depth (D_i) taken as design variables and expressing the cross-section properties in terms of B_i and D_i, the modal displacement $u_{j,\mathrm{member}}^{(n)}$ shown in (15) can be simplified as

$$u_{j,\mathrm{member}}^{(n)}(B_i,D_i)=\sum_{i=1}^{N_i}\left(\frac{C_{1ij}^{(n)}}{B_iD_i}+\frac{C_{2ij}^{(n)}}{B_iD_i^3}+\frac{C_{3ij}^{(n)}}{B_i^3D_i}\right) \tag{19}$$

where

$$C_{1ij}^{(n)}=\int_0^{L_i}\left(\frac{F_X^{(n)}f_{Xj}}{E}+\frac{F_Y^{(n)}f_{Yj}+F_Z^{(n)}f_{Zj}}{5G/6}\right)_i\mathrm{d}x \tag{20a}$$

$$C_{2ij}^{(n)}=\int_0^{L_i}\left(\frac{M_Z^{(n)}m_{Zj}}{E/12}\right)_i\mathrm{d}x;\ C_{3ij}^{(n)}=\int_0^{L_i}\left(\frac{M_X^{(n)}m_{Xj}}{G\kappa}+\frac{M_Y^{(n)}m_{Yj}}{E/12}\right)_i\mathrm{d}x \tag{20b}$$

Once the explicit modal story displacement is formulated, the maximum value of the interstory drifts can be expressed by combination rules. One general and accurate combination rule, the complete quadratic combination (CQC) rule, has been widely used. Using the CQC rule, the interstory drift, Δu_j, can be then determined by the modal drifts given in (16) and (19) as

$$\left[\Delta u_j\right]_{\mathrm{CQC}}=\sqrt{\sum_{n=1}^{N_n}\sum_{m=1}^{N_n}\rho_{nm}\times\Delta u_j^{(n)}\times\Delta u_j^{(m)}} \tag{21}$$

where N_n denotes the total number of modes considered in the response spectrum analysis, and the modal correlation coefficient ρ_{nm} is determined (Chopra 1995) by

$$\rho_{nm}=\frac{8\sqrt{\zeta_n\zeta_m}(\zeta_n+\beta_{nm}\zeta_m)\beta_{nm}^{3/2}}{\left(1-\beta_{nm}^2\right)^2+4\zeta_n\zeta_m\beta_{nm}\left(1+\beta_{nm}^2\right)+4\left(\zeta_n^2+\zeta_m^2\right)\beta_{nm}^2} \tag{22}$$

where

$$\beta_{nm}=\omega_n/\omega_m\le 1 \tag{23}$$

In (22), ζ_n and ζ_m are the nth and mth modal damping ratios; ρ_{nm}=ρ_{mn} when ζ_n=ζ_m; ρ_{nm}=1 when n=m. For structures with well-separated natural frequencies, the modal correlation coefficient ρ_{nm} vanishes, and thus the combination rule CQC is the same as another combination rule widely used—the square root of the sum of the squares.

2.2.2 Explicit formulation of the design problem

Based on the explicit expressions in (16), (19), and (21), the base-isolated structural design optimization problem can be expressed in terms of the design variables, $K_{\mathrm{eff},b}^{\mathrm{h}}$, B_i, and D_i, as

Minimize:

$$F\left(K_{\mathrm{eff},b}^{\mathrm{h}},B_i,D_i\right)=\sum_{b=1}^{N_b}\left(m_1K_{\mathrm{eff},b}^{\mathrm{h}}+m_2\right)+\sum_{i=1}^{N_i}w_iB_iD_i \tag{24}$$

subject to:

1. For the base isolation system,

$$g_j\left(K_{\mathrm{eff},b}^{\mathrm{h}}\right)=u_0^L\left[\sum_{b=1}^{N_b}\left(\frac{C_{0b0}^{(1)}}{K_{\mathrm{eff},b}^{\mathrm{h}}}\right)\right]^{-1}\le 1 \tag{25}$$

$$(j=N_j+1)$$

$$g_j\left(K_{\mathrm{eff},b}^{\mathrm{h}}\right)=u_0^U\sqrt{\sum_{n=1}^{N_n}\sum_{m=1}^{N_m}\rho_{nm}\sum_{b=1}^{N_b}\left(\frac{C_{0b0}^{(n)}}{K_{\mathrm{eff},b}^{\mathrm{h}}}\right)\sum_{b=1}^{N_b}\left(\frac{C_{0b0}^{(m)}}{K_{\mathrm{eff},b}^{\mathrm{h}}}\right)}\le 1 \tag{26}$$

$$(j=N_j+2)$$

2. For the superstructure system,

$$g_j\left(K_{\mathrm{eff},b}^{\mathrm{h}},B_i,D_i\right)=\frac{1}{u_j^U}\sqrt{\sum_{n=1}^{N_n}\sum_{m=1}^{N_m}\rho_{nm}\left[\sum_{b=1}^{N_b}\frac{\Delta C_{0bj}^{(n)}}{K_{\mathrm{eff},b}^{\mathrm{h}}}+\sum_{i=1}^{N_i}\left(\frac{\Delta C_{1ij}^{(n)}}{B_iD_i}+\frac{\Delta C_{2ij}^{(n)}}{B_iD_i^3}+\frac{\Delta C_{3ij}^{(n)}}{B_i^3D_i}\right)\right]\left[\sum_{b=1}^{N_b}\frac{\Delta C_{0bj}^{(m)}}{K_{\mathrm{eff},b}^{\mathrm{h}}}+\sum_{i=1}^{N_i}\left(\frac{\Delta C_{1ij}^{(m)}}{B_iD_i}+\frac{\Delta C_{2ij}^{(m)}}{B_iD_i^3}+\frac{\Delta C_{3ij}^{(m)}}{B_i^3D_i}\right)\right]}\le 1\ \left(j=1,2,\ldots,N_j\right) \tag{27}$$

$$K_{\text{eff},b}^{\text{h},L} \le K_{\text{eff},b}^{\text{h}} \le K_{\text{eff},b}^{\text{h},U} (b = 1, 2, \ldots, N_b) \tag{28a}$$

$$B_i^L \le B_i \le B_i^U;\ D_i^L \le D_i \le D_i^U (i = 1, 2, \ldots, N_i) \tag{28b}$$

Equation (24) defines the total construction cost function F, which contains the concrete cost of the superstructure system and the isolator cost of isolation system. Equations (25) and (26) define the lateral displacement constraints at the base story; the subscript j represents the jth design constraints (j=1,2,…N_j+2); u_0^L is the allowable minimum displacement limit of the base story, determined by (8); u_0^L is the allowable maximum displacement limit of the base story, captured from deformation capacity of individual isolator. Equation (27) defines a set of interstory drift constraints at the two adjacent jth and $j-1$th floor levels for the superstructure; u_j^U is the allowable jth story drift limit value. Equations (28a, b) define the bounds of design variables.

3 Optimality criteria algorithm and design procedure

3.1 Optimality criteria algorithm

Once the design optimization problem is explicitly expressed in terms of design variables, the next task is to adopt a suitable method for solving the problem. A rigorously derived OC approach is adopted in this study because of its superior numerical efficiency for the design of large-scale building structures (Chan et al. 1995; Zou 2002; Zou and Chan 2005a). Specifically, not does only this approach have a weak dependence on the size of the structure and the number of design variables, but also its convergence does not depend on the starting design. In this approach, a set of necessary optimality conditions for the optimal design is first derived, and a recursive algorithm is then applied to achieve indirectly the optimum by satisfying the optimality conditions (Chan et al. 1995; Zou 2002; Zou and Chan 2005a).

In classical optimization theory, the necessary OC for the constrained optimal design problem, (24) to (27), can be obtained indirectly by first converting the constrained problem to an unconstrained Lagrangian function and then solving for the stationary condition of Lagrangian function L. By temporarily omitting the sizing constraints in (28a, b), the unconstrained Lagrangian function, L, can be formulated as

$$L\left(K_{\text{eff},b}^{\text{h}}, B_i, D_i, \lambda_j\right) = F\left(K_{\text{eff},b}^{\text{h}}, B_i, D_i\right) + \sum_{j=1}^{N_j+2} \lambda_j g_j\left(K_{\text{eff},b}^{\text{h}}, B_i, D_i\right) \tag{29}$$

where a series of λ_j are called the Lagrangian multipliers corresponding to the active constraints.

By differentiating (29) with respect to the design variables and setting the derivatives to zero, the stationary conditions of the Lagrangian function are shown as

$$\frac{\partial L}{\partial K_{\text{eff},b}^{\text{h}}} = 0 \Rightarrow \frac{\partial F}{\partial K_{\text{eff},b}^{\text{h}}} + \sum_{j=1}^{N_j+2} \lambda_j \frac{\partial g_j}{\partial K_{\text{eff},b}^{\text{h}}} = 0 \quad (b = 1, 2, \ldots, N_b) \tag{30a}$$

$$\frac{\partial L}{\partial B_i} = 0 \Rightarrow \frac{\partial F}{\partial B_i} + \sum_{j=1}^{N_j+2} \lambda_j \frac{\partial g_j}{\partial B_i} = 0; \tag{30b}$$

$$\frac{\partial L}{\partial D_i} = 0 \Rightarrow \frac{\partial F}{\partial D_i} + \sum_{j=1}^{N_j+2} \lambda_j \frac{\partial g_j}{\partial D_i} = 0 \quad (i = 1, 2, \ldots, N_i) \tag{30c}$$

Based on (30a, 30b), a linear recursive relation to resize design variables $K_{\text{eff},b}^{\text{h}}$, B_i, and D_i can be given as

$$K_{\text{eff},b}^{\text{h},\nu+1} = K_{\text{eff},b}^{\text{h},\nu}\left[1 + \frac{1}{\eta}\left(\frac{\sum_{j=1}^{N_j+2} \frac{\partial g_j}{\partial K_{\text{eff},b}^{\text{h}}} \lambda_j}{\frac{\partial F}{\partial K_{\text{eff},b}^{\text{h}}}} - 1\right)\right] \text{ for active } K_{\text{eff},b}^{\text{h}} \tag{31a}$$

$$B_i^{\nu+1} = B_i^{\nu}\left[1 + \frac{1}{\eta}\left(\frac{\sum_{j=1}^{N_j+2} \frac{\partial g_j}{\partial B_i} \lambda_j}{\frac{\partial F}{\partial B_i}} - 1\right)\right] \text{ for active } B_i \tag{31b}$$

$$D_i^{\nu+1} = D_i^{\nu}\left[1 + \frac{1}{\eta}\left(\frac{\sum_{j=1}^{N_j+2} \frac{\partial g_j}{\partial D_i} \lambda_j}{\frac{\partial F}{\partial D_i}} - 1\right)\right] \text{ for active } D_i \tag{31c}$$

where $\frac{\partial F}{\partial K_{\text{eff},b}^{\text{h}}}$, $\frac{\partial F}{\partial B_i}$, $\frac{\partial F}{\partial D_i}$ can be obtained by differentiating (24) with respect to the corresponding design variables; $\frac{\partial g_j}{\partial K_{\text{eff},b}^{\text{h}}}$ can be obtained by differentiating (27) when j=1,2,…, N_j, (25) when j=N_j+1, and (26) when j=N_j+2; $\frac{\partial g_j}{\partial B_i}$ and $\frac{\partial g_j}{\partial D_i}$ can be determined from (27); ν denotes the current iteration number, and η is a relaxation parameter that can be adaptively adjusted to control the rate of convergence. Before (31a, b, c) can be utilized to find the variables $K_{\text{eff},b}^{\text{h}}$, B_i, and D_i, the Lagrange multipliers, λ_j, must first be determined. By considering the sensitivity of the kth constraint because of the change in the design variables, $K_{\text{eff},b}^{\text{h}}$, B_i, and D_i, the following simultaneous equation can

then be established to solve for the set of Lagrangian multipliers (Zou 2002):

$$\sum_{j=1}^{N_j+2}\lambda_j^{\nu}\left(\sum_{b=1}^{N_b}\frac{K_{\mathrm{eff,b}}^{\mathrm{h}}\frac{\partial g_k}{\partial K_{\mathrm{eff,b}}^{\mathrm{h}}}\frac{\partial g_j}{\partial K_{\mathrm{eff,b}}^{\mathrm{h}}}}{\frac{\partial F}{\partial K_{\mathrm{eff,b}}^{\mathrm{h}}}}+\sum_{i=1}^{N_i}\frac{B_i\frac{\partial g_k}{\partial B_i}\frac{\partial g_j}{\partial B_i}}{\frac{\partial F}{\partial B_i}}+\sum_{i=1}^{N_i}\frac{D_i\frac{\partial g_k}{\partial D_i}\frac{\partial g_j}{\partial D_i}}{\frac{\partial F}{\partial D_i}}\right)_{\nu} \quad (32)$$
$$=-\left(\sum_{b=1}^{N_b}K_{\mathrm{eff,b}}^{\mathrm{h}}\frac{\partial g_k}{\partial K_{\mathrm{eff,b}}^{\mathrm{h}}}+\sum_{i=1}^{N_i}B_i\frac{\partial g_k}{\partial B_i}+\sum_{i=1}^{N_i}D_i\frac{\partial g_k}{\partial D_i}\right)_{\nu}-\eta\left(1-g_k^{\nu}\right)$$
$$(k=1,2,\ldots,N_j+2)$$

Equations (31a, b, c) for the sizing variables and (32) for Lagrange multipliers form the basis of the iterative OC method for the solution of the optimal design problem, (24) to (28a, b). By successively applying the recursive optimization iteration until the convergence of $K_{\mathrm{eff},b}^{\mathrm{h},\nu}$, B_i^{ν}, and D_i^{ν} as well as λ_j^{ν} occurs, then the continuous optimal solution for the design problem, (24) to (28a, b), are then found.

For the case of a statically indeterminate structure, the explicit design formulation, (24) to (28a, b), is only approximate because any changes in the member sizes will cause a redistribution of the internal forces and a change in the natural frequencies of the building structure. Consequently, it is necessary to reanalyze the structure for the updated sizes after each OC optimization process and to reapply the iterative analysis and design optimization processes until the solution convergence is achieved.

3.2 Procedure of seismic optimal design

The automated optimal design procedure for base-isolated multistory building structures is outlined as follows.

1. Assume initial member sizes of the superstructure, identify the initial number and size of base isolators for the isolation system, and determine their lower and upper size bounds.
2. Determine the target period of the isolation system, $T_{B.}$
3. Choose the type of isolators and establish the cost function like (5b) and (5c).
4. Compute the total effective damping ratio, ζ_B, of the isolation system by (2) and the corresponding spectral acceleration, $S_a^{(1)}(T_B,\zeta_B)$, by (9).
5. Carry out the spectrum analysis of the structure with the damping ratio, ζ_{B}, (using commercially available software package) to determine actual internal forces and moments of all members and isolators and to obtain the first modal participation factor, $\Gamma^{(1)}$, as well as the amplitude of the first mode at base story, $\phi_0^{(1)}$.
6. Determine the minimum and maximum displacement limits, u_0^L and u_0^U for the base isolation system at the base floor level by (8) and (10b), respectively.
7. Apply virtual loads to the structure and perform static virtual load analyses to determine virtual internal forces and moments of all members and isolators.
8. Establish the expicit formulation of the optimal design problem (24) to (28a, b) for the lateral drift constraints of the superstructure and the isolation system.
9. Apply the recursive OC optimization algorithm to calculate the Lagrange multipliers, λ_{j} by (32) and then to resize the design variables $K_{\mathrm{eff},b}^{\mathrm{h}}$, B_i, and D_i by (31a, b, c), and determine the optimal total cost of the member sizes of the building structure and the base isolation system by (24).
10. Check the convergence of the objective function (24). If the total costs of the base isolated structure for two successive design cycles are within 0.5%, the optimal design solution is deemed to converge and then the design is terminated; otherwise, return to step 4 for the next design cycle.

4 Illustrative example

4.1 Design problem

A ten-story, two-bay planar frame without and with base isolation is used to illustrate the optimal design method for the minimum cost design subject to spectral drift constraints. The structural geometries of the fixed-base and base-isolated buildings are given in Figs. 5a and b, respectively. The purpose of this example case is also to compare the isolation effect of the optimal base-isolated structure with the optimal fixed-base structure. The mass of each story is assumed to be 50 tonnes. The structure is subjected to the lateral loads derived from the seismic design response spectrum with the peak acceleration of 0.32 g and with the damping ratio of 5% in accordance with the Chinese seismic design code (National Standard of the People's Republic of China 1994) as shown in Fig. 6.

To study the trend of optimal member sizes, this example does not impose any upper size bounds on the depths and widths of all element sections. Based on typical buildability requirements, lower bound depths are 300 mm for all members, and lower bound widths are 250 and 300 mm for beams and columns, respectively. To commence the optimization process, the framework is first analyzed with the members arbitrarily taken to have the initial sizes 300×300 mm (width×depth) for columns and 250×350 mm for beams, respectively. Members of the structure are grouped together to have the same sizes for every two stories as shown in Table 2. There are three isolators for use, denoted by BI_1 and grouped together. Their bounds and initial values of horizontal stiffness are shown in Table 3. Vertical stiffness is assumed to be 1,000 times that of the horizontal stiffness and cylindrical rubber isolators are used in this example. For both the fixed-base and base-isolated structures, an allowable interstory drift ratio limit is assumed to

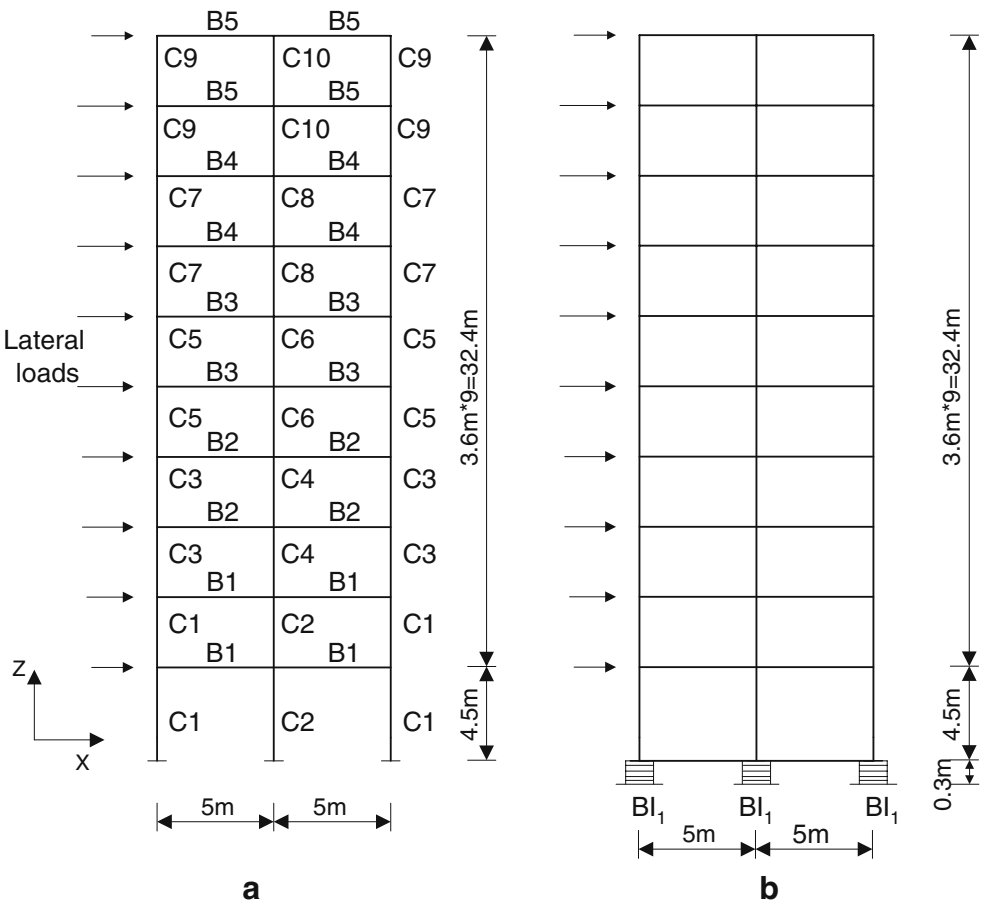

Fig. 5 **a**, **b** A ten-story, two-bay concrete frame with and without isolation

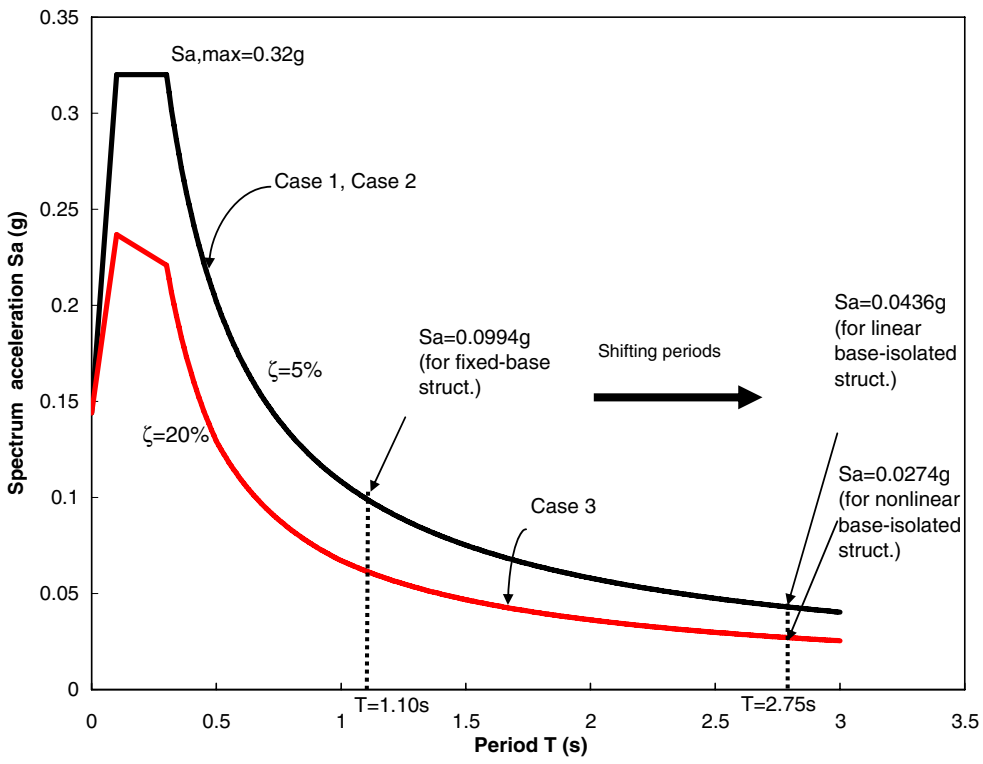

Fig. 6 Seismic design response spectra

Table 2 Initial and optimal member sizes

Isolated structure	Element type	Story level	Member group	Initial sizes		Case 1		Case 2			Case 3		
						Optimal sizes		Optimal sizes		Ratio	Optimal sizes		Ratio
				Width (mm) (1)	Depth (mm) (2)	Width (mm) (3)	Depth (mm) (4)	Width (mm) (5)	Depth (mm) (6)	(3)/(6) (7)	Width (mm) (8)	Depth (mm) (9)	(3)/(9) (10)
Superstructure	Columns	9th–10th	C9	300	300	300	458	300	350	1.3	300	350	1.3
			C10	300	300	300	683	300	419	1.6	300	350	2.0
		7th–8th	C7	300	300	300	519	300	414	1.3	300	354	1.5
			C8	300	300	300	790	300	590	1.3	300	529	1.5
		5th–6th	C5	300	300	300	604	300	461	1.3	300	376	1.6
			C6	300	300	300	812	300	644	1.3	300	556	1.5
		3rd–4th	C3	300	300	300	682	300	505	1.4	300	407	1.7
			C4	300	300	300	840	300	666	1.3	300	574	1.5
		1st–2nd	C1	300	300	300	887	300	605	1.5	300	485	1.8
			C2	300	300	300	785	300	750	1.0	300	648	1.2
	Beams	9th–10th	B5	250	350	250	583	250	450	1.3	250	450	1.3
		7th–8th	B4	250	350	250	815	250	559	1.5	250	450	1.8
		5th–6th	B3	250	350	250	866	250	673	1.3	250	584	1.5
		3rd–4th	B2	250	350	250	903	250	713	1.3	250	604	1.5
		1st–2nd	B1	250	350	250	883	250	764	1.2	250	649	1.4

be 1/800. In determining the combined modal drift quantities, the first five modal responses are combined. The design process is considered to converge when the costs of two successive design cycles are within 0.5%. Linear isolators GZP-V5A and nonlinear isolators GZY-V5A are used, whose cost functions are shown in (5b) and (5c).

Three cases are considered in this example. Case 1 commences the optimal design of the fixed-base structure with a 5% damping ratio. The fixed-base structural optimization method proposed in Zou (2002), Zou and Chan (2005a) is used to produce an optimal design of the building with the natural period of 1.1 s. The target period of 2.75 s, which is approximately 2.5 times of the optimized fixed-base structure, is desired for the base-isolated building. Case 2 is defined that linear isolators with a 5% damping ratio are used, resulting in a 5% effective damping of the isolation system. Case 3 is defined that nonlinear isolators with a 20% damping ratio are adopted, and thus the effective damping of the isolation system is 20%. According to (7), the allowable minimum displacement limit of the base story can be approximately computed, and it is equal to 0.025 m for case 2 and 0.056 m for case 3. Herein, cases 2 and 3 are used to study and exhibit damping effect and isolation effect for a linearly isolated structure and a bilinearly isolated structure.

4.2 Comparison of fixed-base and base-isolated structures

4.2.1 Design history

Figure 7 presents the design histories of total construction cost with and without base isolation for the specified earthquake loading. Rapid and steady convergence to the optimal design is found for the framework. This is due to the fact that the member force distribution for such structure is somewhat insensitive to the changes in member sizes and isolator stiffnesses. It is further found that the optimal design of the base-isolated structure converges faster than that of the fixed-base system. The main reason is that the spectrum acceleration of the isolated structure is located in a smooth long period band in the spectrum as illustrated in Fig. 6 so that the change in earthquake loads is less sensitive to the change in the period of the structure.

Compared with the concrete cost of US$12,076 for the optimized fixed-base structure, the total cost of US$9,686, containing the concrete cost of US$7,459 and the isolator cost of US$2,227 for the optimized nonlinearly isolated structure, is found to be much cheaper, whereas the total cost of US$16,896, containing the concrete cost of US $8,777 and the isolator cost of US$8,119 for the optimized linearly isolated structure, is found to be more expensive. About 2.7 and 3.8% of concrete cost are reduced, respectively, in cases 2 and 3 compared with the optimized

Table 3 Isolator stiffnesses

Isolated structure	Element type	Story level	Member group	Stiffness bounds (kN/m)	Case 2		Case 3	
					Initial stiffness (kN/m)	Optimal stiffness (kN/m)	Initial stiffness (kN/m)	Optimal stiffness (kN/m)
Isolation	solator	Base	BI_1	610–2,480	610	1,353	860	1,790

fixed-base structure in case 1. As mentioned previously, a major advantage of using seismic isolation is that by lengthening the fundamental period of the structure, spectral acceleration is shifted from large to small values. It can be observed from the design spectrum (see Fig. 6) that the spectrum acceleration value of $0.0274\times g$ for the optimized, nonlinearly isolated structure is one third of $0.0994\times g$ (i.e., the spectral acceleration of the optimized fixed-base structure), while the spectral acceleration value of $0.0436\times g$ for the optimized, linearly isolated structure is about one half of $0.0994\times g$. The acceleration reduction causes a significant decrease in earthquake loads so that the structural internal forces as well as member sizes are reduced, resulting in the great reduction of the concrete cost of the superstructure. Thus, the concrete costs in cases 2 and 3 are less than that in case 1, and furthermore, the concrete cost in case 3 is less than that in case 2 because of the reduction in earthquake loads by increasing the damping ratio.

When the horizontal effective stiffness, $K_{\text{eff}}^{\text{h}}$, changes within the range of $450\text{kN/m} \le K_{\text{eff}}^{\text{h}} < 2,755\ \text{kN/m}$, $K_{\text{eff}}^{\text{h}}$ of a linear isolator is lower than that of a nonlinear isolator under the same dimensions of isolators, while the cost of a linear isolator is much higher than that of a nonlinear isolator. In case 2, each linear isolator must provide a high value of $K_{\text{eff}}^{\text{h}}$ in order that this base-isolated structure can reach the same target period of 2.75 s as that in case 3. This high value of $K_{\text{eff}}^{\text{h}}$ results in a great increase in the isolator cost, and thereby, the sum of the concrete cost and isolator cost in case 2 is still greater than the cost of the fixed-base structure even if isolators are used. However, the cost of nonlinear isolators in case 3 is relatively not expensive because of the low value of $K_{\text{eff}}^{\text{h}}$, and so the total cost is less than that in case 1.

4.2.2 Design variables

Table 2 shows the initial and optimal member sizes for both the fixed-base and base-isolated structures. The distribution of section sizes indicates that all member widths take the minimum width limit of 300 mm for columns and 250 mm for beams for both of structures. However, the depths of all members are found to decrease gradually as the framework rises in height. That is to say, if the sizes of the two-dimensional frame members need to be increased to maximize the structural stiffness and minimize the material costs, it would be more cost effective to increase the depths of these members rather than their widths. Moreover, the member depths of the isolated structure are much smaller than those of the fixed-base structure. Specifically, it is seen from columns 7 and 10 that the ratio of the member depth for the fixed-base structure over the depth for the isolated structure is approximately equal to 1.3 in case 2 and 1.5 in

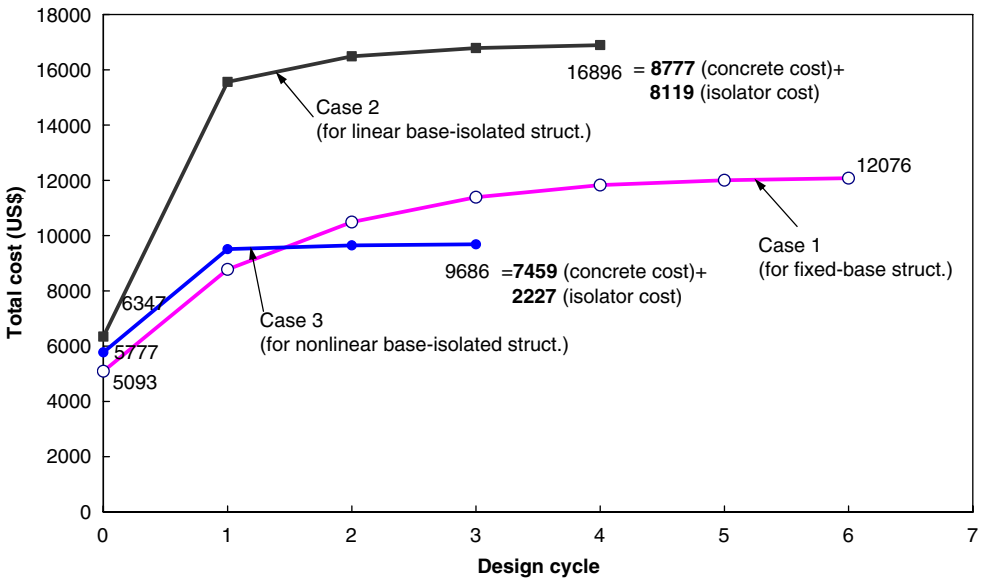

Fig. 7 Design histories of the total construction cost

Table 4 Natural periods of vibration for optimized structures

Mode	Case 1 period (s)	Case 2 period (s)	Case 3 period (s)
1	1.057	2.756	2.752
2	0.410	0.882	0.997
3	0.236	0.451	0.533
4	0.160	0.295	0.355
5	0.119	0.216	0.267

case 3. This is due to the fact that the spectrum acceleration is proportional to the earthquake load, which is also proportional to the flexural moment of inertia of a member section and then the cube of the member depth. In addition, Table 3 shows the initial and optimal horizontal effective stiffnesses of each isolator in cases 2 and 3. It is found that optimal effective stiffness is higher than the initial one for each isolator. This can be explained by the fact that the initial stiffness is indeed so small that excessive base story displacement occurs, and so it is improved by the optimization process.

4.2.3 Vibration period and participation factors

Table 4 presents the natural vibration periods of the optimized structure with and without base isolation. In the first structural mode, the natural period of 1.057 s for the optimized fixed-base structure is lengthened to 2.756 s for the linear base-isolated structure and 2.752 s for the nonlinear base-isolated structure. Clearly, the isolation system has a large effect on the natural period of the first structural mode, but a decreasing effect on the higher mode periods as shown in Table 3. In addition, the fundamental natural periods of the optimized structures (i.e., 2.756 s for case 2 and 2.752 s for case 3) are very close to the target period of 2.75 s.

Table 5 presents the effective mass factors of the optimized structure with and without base isolation for the first five modes. These effective mass factors provide an insight into how much each mode mass contribution is to the response. It is found that the first mode effective mass factor of the structure with base isolation is greater than that without base isolation. This is because the isolation system has a larger effect on the first mode response, which dominates the building response.

Table 5 Comparison of effective mass factors for optimized structures

Mode	Case 1 (%)	Case 2 (%)	Case 3 (%)
1	77.64	96.97	96.77
2	14.65	2.73	2.92
3	4.81	0.22	0.23
4	1.77	0.05	0.05
5	0.54	0.02	0.02

4.2.4 Shear forces

Table 6 shows the cumulative story shear distribution for the optimized structure with and without base isolation. It is evident that the story shear on the fixed-base frame is found to be much larger than that on the base-isolated structure (i.e., approximately twice of fixed-base shear force in case 2 and three times in case 3, as shown in columns 3 and 5 of Table 6). As shown by the spectrum in Fig. 6, compared with the natural period of 1.1 s for the fixed-base structure, this longer natural period of 2.75 s for the base isolated structure reduces the spectrum acceleration value from $0.0994\times g$ in case 1 to $0.0436\times g$ in case 2 or $0.0274\times g$ in case 3, and consequently, the applied earthquake loads and base shear of the structure are reduced. Thereby, the isolation system is effective in reducing earthquake loads even if the system damping is low (i.e., in case 2). Besides, further compared to columns 3 and 5, it is found that the shear forces in case 3 are more significantly reduced than those in case 2. It indicates that damping is beneficial in further reducing the forces in the structure.

4.2.5 Lateral deformation

The initial and final interstory drift responses for both the fixed-base and base-isolated structures are shown in Figs. 8a–c. Initially, the interstory drift constraints are substantially violated for the structure with and without the isolation system. After the optimization, no violation in interstory drift can be found. The optimized structure is found to be stiffened and most of the lateral drifts are very close to the allowable interstory drift ratio limit of 1/800. It implies that the OC technique developed herein is able to automatically distribute the structural stiffness to satisfy the specified design criteria.

Table 6 Story shear forces for optimized structures

Story level	Case 1	Case 2		Case 3	
	Shear (kN) (1)	Shear (kN) (2)	Ratio (1)/(2) (3)	Shear (kN) (4)	Ratio (1)/(4) (5)
10	117.000	32.760	3.6	22.800	5.1
9	185.560	60.640	3.1	40.980	4.5
8	227.100	84.600	2.7	56.110	4.0
7	261.490	106.570	2.5	69.620	3.8
6	291.200	126.720	2.3	81.810	3.6
5	319.930	145.690	2.2	93.140	3.4
4	348.430	163.570	2.1	103.460	3.4
3	376.240	180.650	2.1	112.950	3.3
2	402.370	197.040	2.0	121.660	3.3
1	426.700	213.020	2.0	129.900	3.3

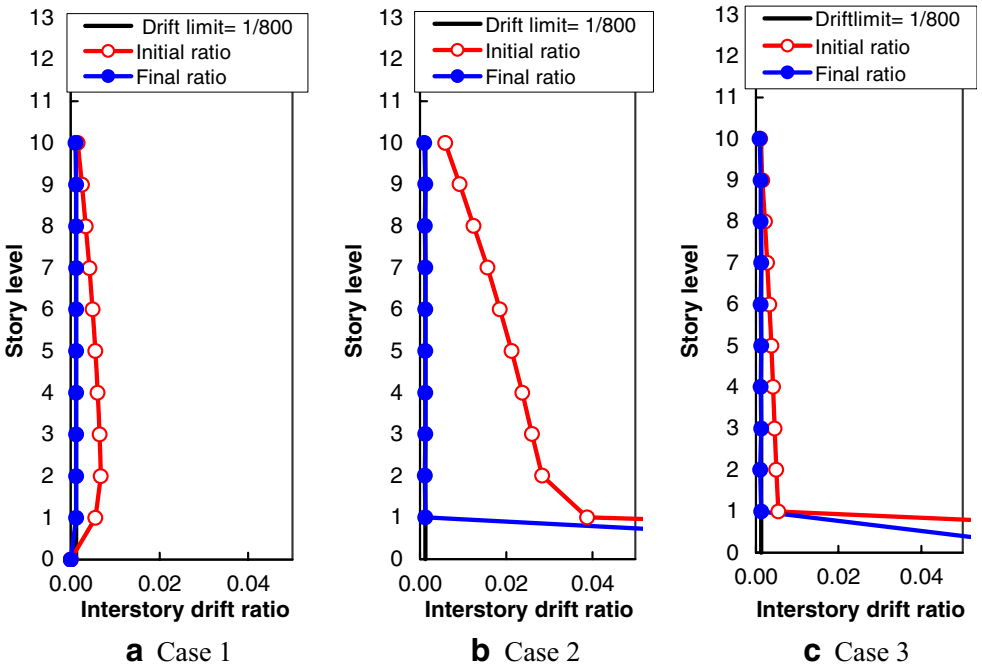

Fig. 8 a–c Initial and final interstory drift ratios

Compared to both cases 2 and 3, it is found from Figs. 8b–c that although initial interstory drifts and lateral displacements of the superstructure are different from each other, the final responses in case 2 are almost the same as those in case 3, and most of the interstory drift constraints become active at optimum. It is explained that the superstructures in the two cases have the same design constraints as well as allowable interstory drift ratio limits, although the allowable lateral displacement limits at the base story are different.

Table 7 shows the initial and final lateral displacement at the base story in cases 2 and 3. It is found that the lateral displacement at the base story is very close to the corresponding allowable limit at optimum. It indicates that this displacement constraint is active. Meanwhile, under the condition that the isolated structure reaches the same target period of 2.75 s, lateral displacement in case 3 is less than that in case 2. This is due to the fact that the isolation system in case 3 has a higher damping than that in case 2, whereas higher damping can reduce the lateral displacement than the lower damping. This verifies that damping is beneficial not only in further reducing the forces in the structure but also in reducing the deformation in the isolation system. Besides, such a result shows that linear base-isolation systems could cause larger displacements of the ground floor of the building, and thus the use of a nonlinear isolator, assuring high-energy dissipation when working out of linear range, should be highly recommended.

5 Concluding remarks

The developed design optimization technique can provide an efficient design approach for an isolated structure through integrating the response spectrum analysis with optimization techniques. Especially, this technique is capable of achieving the ideal drift performance design, the target period, and the optimal balance between the superstructure cost and the isolation system cost by simultaneously optimizing both the superstructure and the base isolation, which are as a whole.

It has been exhibited from the illustrative example that the proposed technique for both the fixed-base and base-isolated building structures converges rapidly and steadily. Furthermore, it indicates that using the base isolators can greatly reduce the concrete cost of the superstructure while

Table 7 Lateral displacement at base story

Story level	Case 2			Case 3		
	Limit value (m)	Initial displacement (m)	Final displacement (m)	Limit value (m)	Initial displacement (m)	Final displacement (m)
Base	0.056	0.111	0.056	0.025	0.070	0.025

the isolator cost is dependent on isolator market price. From the structural characteristics and the response features of the two structures, it is also evident that when a conventional earthquake-resistant system is used, the seismic forces and interstory drifts are larger than those occurring when a seismic isolation system is used. Besides, it has been indicated that the proposed technique has an ability to drive an initial structural natural period to a target period in the optimization process. More importantly, the OC technique developed is able to optimize the base-isolated structure so as to automatically distribute member sizes and isolator-effective stiffnesses to satisfy all code-specified design performance criteria.

The integrated optimal design methodology developed in this paper provides a powerful computer-based technique to automate the practical design of base-isolated concrete building structures. This study represents the starting point for future research on optimizing base-isolated building design using full nonlinear analysis such as nonlinear time history analysis.

Acknowledgments The author would acknowledge the thoughtful suggestions and support from Prof. C. M. Chan of the Department of Civil Engineering, the Hong Kong University of Science and Technology. The author also would acknowledge the generous assistance provided by Prof. Fu-Lin Zhou and Dr. Zhong-Gen Xu of Guangzhou University, P.R. China, and Mr. Shou-Long Feng from Shantou Vibro Tech Industrial and Development, P.R. China.

References

Booth E (ed) (1994) Concrete structures in earthquake regions: design and analysis Longman, Australia

Ceccoli C, Mazzotti C, Savoia M (1999) Non-linear seismic analysis of base-isolated RC frame structures. Earthq Eng Struct Dyn 28: 633–653

Chan CM (2001) Optimal lateral stiffness design of tall buildings of mixed steel and concrete construction. Struct Des Tall Build 10 (3):155–177

Chan CM, Zou XK (2004) Elastic and inelastic drift performance optimization for reinforced concrete building under earthquake loads. Earthq Eng Struct Dyn 33(8):929–950

Chan CM, Grierson DE, Sherbourne AN (1995) Automatic optimal design of tall steel building frameworks. J Struct Eng 121(5):88–845

Cheng FY, Li D (1996) Multiobjective optimization of structures with and without control. J Guid Control Dyn 19(2):393–397 March–April

Chopra AK (1995) Dynamics of structures: theory and applications to earthquake engineering. Prentice-Hall, Englewood Cliffs, NJ

Constantinou AM, Tadjbakhsh A (1985) Optimum characteristics of isolated structures. J Struct Eng 111:2733–2750

Fujita S, Furuya O, Fujita T (1994) Dynamic tests on high damping rubber damper for vibration control of tall buildings. FA2–3; First World Conference on Structural Control, Los Angeles, CA, USA, 3–5 August

Hart GC, Wong K (2000) Structural dynamics for structural engineers. Wiley, New York

Inaudi JA, Kelly JM (1993) Optimum damping in linear isolation systems. Earthq Eng Struct Dyn 22:583–598

International Conference of Building Officials (1997) Earthquake regulations for seismic-isolated structures (Appendix, Chapter 16). Uniform Building Code, Whittier, CA

Kelly JM (1997) Earthquake-resistant design with rubber, 2nd edn. Springer, New York

Kelly JM (1999a) The role of damping in seismic isolation. Earthq Eng Struct Dyn 28:3–20

Kelly JM (1999b) Design of seismic isolated structures from theory to practice. Wiley, New York

Komodromos P (2000) Seismic isolation for earthquake resistant structures. WIT, Southampton, UK

National Standard of the People's Republic of China (1994) Chinese code for seismic design buildings (GBJ11–89). New World, Beijing, China

Paulay T, Priestley MJN (1992) Seismic design of reinforced concrete and masonry buildings. Wiley, New York

Shenton HW III, Lin AN (1993) J Struct Engng ASCE 119:2959–2968

Skinner RI, Robinson WH, McVerry GH (1993) An introduction to seismic isolation. Wiley, New York

Zhou FL (1997) Seismic control of structures. Chinese Seismic, China

Zou XK (2002) Optimal seismic performance-based design of reinforced concrete buildings. Ph.D. dissertation, Hong Kong University of Science and Technology

Zou XK, Chan CM (2001) Optimal drift performance design of base isolated buildings subject to earthquake loads. In: OPTI 2001-Seventh International Conference on Computer Aided Optimum Design of Structures, Bologna, Italy, pp 369–378, May

Zou XK, Chan CM (2004) Integrated time history analysis and performance-based design optimization of base-isolated concrete buildings. In: Proc. 13th World Conference on Earthquake Engineering, Vancouver, Canada, Aug. 1–6, Paper no 1314

Zou XK, Chan CM (2005a) An optimal resizing technique for seismic drift design of concrete buildings subjected to response spectrum and time history loadings. Comput Struct 83:1689–1704

Zou XK, Chan CM (2005b) Optimal seismic performance-based design of reinforced concrete buildings using nonlinear pushover analysis. Eng Struct 27:1289–1302

Zou XK (2006) Seismic performance design of concrete buildings with life-cycle cost optimization. Proc., 9th International Symposium on Structural Engineering for Young Experts (ISSEYE-9), Fuzhou & Xiamen, P. R. China, pp 768–774, August

Zou XK, Chan CM, Li G, Wang Q (2007a) Multi-objective optimization for performance-based design of reinforced concrete frames. J Struct Eng 133(10):1462–1474

Zou XK, Teng JG, Lorenzis LD, Xia SH (2007b) Optimal performance-based seismic retrofit design of RC frames using FRP confinement. Composites B Eng 38:584–597